# An Omnidirectional Biomechanical Energy Harvesting (OBEH) Sidewalk Block for a Self-Generative Power Grid in a Smart City

**Jinshi Cui[1,*], Heonjun Yoon[1,*], and Byeng D. Youn[1,2,#]**

1 Department of Mechanical and Aerospace Engineering, Seoul National University, 1 Gwanak-ro, Gwanak-gu, Seoul, 08826, Republic of Korea
2 Institute of Advanced Machines and Design, Seoul National University, 1 Gwanak-ro, Gwanak-gu, Seoul, 08826, Republic of Korea
# Corresponding Author / E-mail: bdyoun@snu.ac.kr, TEL: +82-2-880-1919
ORCID: 0000-0003-0135-3660
*Jinshi Cui and Heonjun Yoon contributed equally to this work as the first author

*Energy harvesting, which converts ambient, otherwise wasted, energy sources into usable electricity, is expected to contribute to the formulation of a self-generating power grid. This type of grid can enable sustainable operation of wireless sensor networks as the "Smart City" vision becomes reality. Human walking is a plentiful mechanical energy source wasted during daily activities. This study aims to develop an omnidirectional biomechanical energy harvesting (OBEH) sidewalk block that is able to generate electricity from human walking. Here, a systematic design framework for the OBEH sidewalk block is presented; it consists of three important ingredients, specifically: (1) extraction of a footstep loading profile from human gait analysis; (2) electroelastically coupled finite element modeling to estimate the transient output responses under the footstep loading profile; and (3) reliability-based design optimization of the OBEH sidewalk block. This study considers two kinds of the inherent randomness, including (1) variability in the material properties and geometry; and (2) uncertainty in the position and direction of the footsteps. It can be concluded from the results that the optimum design of the proposed OBEH sidewalk block enables useful power generation while satisfying the target reliability of fatigue failure in the presence of the inherent randomness.*

## NOMENCLATURE

$T_{ij}$ = Second-rank stress tensor

$S_{kl}$ = Second-rank strain tensor

$c_{ijkl}$ = Fourth-rank elastic modulus tensor

$s_{ijkl}$ = Fourth-rank elastic compliance tensor

$e_{kij}$ = Third-rank piezoelectric constant tensor

$E_k$ = Electric field vector

$D_i$ = Electric displacement vector

$\varepsilon_{ij}$ = Second-rank dielectric permittivity tensor

$C_p$ = Capacitance

$\tau$ = Time constant

$R_L$ = External electrical resistance

$h_p$ = Thickness of the piezoelectric layers

$h_s$ = Thickness of the structural layer

$r_i$ = Inner radius of the annular piezoelectric layers

$r_o$ = Outer radius of the annular piezoelectric layers

$\mathbf{d}$ = Design vector

$\mathbf{X}$ = Random vector

OE = Output energy generated by the piezoelectric layers

G = Performance function against fatigue failure

$\sigma_p$ = Maximum principal stress of the piezoelectric layers

$\sigma_e$ = Fatigue limit of the piezoelectric layers

$P_t$ = Target reliability

$A_p$ = Top surface area of the piezoelectric layer

$I[\bullet]$ = Indicator function

$\Omega_{safe}$ = Safe domain of a design vector space

Springer

# 1. Introduction

With the development of the Internet of Things (IoT), the era of the Smart City is quickly approaching. As wireless sensor networks (WSNs) are essential to monitor space, objects, human beings, and the interactions among them, WSNs are of growing importance in the IoT. However, the powering of wireless sensors still relies on chemical batteries, and the limited lifespan of chemical batteries is a nuisance that hinders wireless sensor use and applications. For successful realization of the Smart City vision, a self-generative power grid must be fulfilled as a countermeasure to eliminate the battery dependency, thereby enabling sustainable operation of WSNs.

Energy harvesting that can convert ambient, otherwise wasted, energy sources into usable electricity has received much attention as a promising solution for a self-generative power grid.[1-5] Among various energy harvesting technologies, piezoelectric energy harvesting involves generating electricity from mechanical energy (e.g., quasi-static forces, vibrations, and impacts), one of the most ubiquitous energy sources, by using piezoelectric materials.[6] When a piezoelectric material is deformed due to an external mechanical stimuli, it produces a charge flow caused by the motion of electric dipoles. This electroelastic phenomenon is called the direct piezoelectric effect.[7,8] Piezoelectric energy harvesting is of great research interest due to its high energy density and ease of installation.[9,10] Thus, advances in piezoelectric energy harvesting are expected to shed light on the potential of self-generative power grids and to bring us closer to the era of the Smart City.

Human walking is a plentiful biomechanical energy source that is wasted during daily activities.[11,12] Many research efforts have been made to turn biomechanical energy available in human daily activities into usable electricity by using piezoelectric materials. Riemer and Shapiro considered heel strikes, center of mass motions, shoulder and elbow joint motions during arm swings, and leg motions (i.e., ankle, knee, and hip motions) as potential biomechanical energy sources during human walking.[13] Shenck et al. explored a method to harness foot strike energy by using lead zirconate titanate (PZT) embedded in a shoe heel.[14] Zhao et al. developed a polyvinylidene difluoride (PVDF) based energy harvester embedded in a shoe insole.[15] Pozzi and Zhu introduced mechanical plucking-based frequency up-conversion so as to permit a piezoelectric energy harvester that scavenges the biomechanical energy of knee-joint motions at its resonance.[16]

However, while these types of approaches are appropriate for powering portable/wearable personal electronics, they cannot readily provide a solution for a self-generative power grid needed for operation of a WSN. As an alternative approach, this study focuses on a sidewalk block concept used for the purpose of biomechanical energy harvesting. The proposed approach generates electricity from footsteps to run low-power traffic systems and/or street lighting. In this concept, when a pedestrian walks, the energy harvesting sidewalk block undergoes deflection upon the vertical force, thereby producing output electric power through the direct piezoelectric effect. Locations where energy harvesting sidewalk blocks can be applied include train stations, airports, and any public place with a large, moving population.

Even though various commercial products (e.g., Pavegen, Waynergy, Innowattech, and Senbool) have been released and installed,

there is still a great need for a systematic framework for designing an energy harvesting sidewalk block that is capable of answering the following three questions of fundamental importance. First, how can human walking characteristics can be incorporated into the design process of an energy harvesting sidewalk block? To the best of authors' knowledge, very little work has theoretically investigated the effect of human gait cycles on the power generation capability of an energy harvesting sidewalk block. Second, how can biomechanical energy raised by human walking be reliably converted into electricity in the presence of the inherent randomness? The inherent randomness considered here includes variability in the system parameters (i.e., the material properties and the geometry) and loading parameters (i.e., the footstep direction and the footstep position). Third, how can the electroelastic behaviors of the energy harvesting sidewalk block be elucidated under transient footstep loading?

This study thus proposes an omnidirectional biomechanical energy harvesting (OBEH) sidewalk block that generates electricity from human walking. In this paper, a systematic framework for developing an OBEH sidewalk block is presented; the framework consists of three important ingredients: (1) extraction of a footstep loading profile from human gait analysis; (2) electroelastically coupled finite element (FE) modeling to estimate the transient output responses under the footstep loading profile; and (3) reliability-based design optimization (RBDO) of the OBEH sidewalk block under physical uncertainty.

The rest of this article is organized as follows. Section 2 provides the conceptual design of the OBEH sidewalk block based on human gait analysis. Section 3 describes the electroelastically coupled FE model of the OBEH sidewalk block under transient footstep loading. Section 4 explains design optimization of the OBEH sidewalk block under physical uncertainty. Finally, the conclusions of this study are outlined in Section 5.

# 2. Principles of the Omnidirectional Biomechanical Energy Harvesting Sidewalk Block

This section is devoted to explanation of the working principles of the proposed OBEH sidewalk block. Section 2.1 presents the extraction of a loading profile from human gait analysis and Section 2.2 describes the configuration of the OBEH sidewalk block.

## 2.1 Human Gait Analysis: Loading Profile

To incorporate the dynamic behavior of human walking into the design of an OBEH sidewalk block, human gait analysis is required to extract a transient vertical loading profile. The human gait cycle refers to the duration from the initial ground contact to the next contact of one foot. The human gait cycle can be divided into the stance and the swing phases.[17] In one gait cycle, the stance phase generally takes up 60% and swing phase accounts for the remaining 40% of the cycle. The stance phase is also called the contact phase, which includes the stages from the 'initial contact' to the 'toe off' of the support foot (orange color), as shown in Fig. 1. The support foot remains in contact with the ground during the stance phase. Therefore, our focus in this study, the stance phase is mainly focused on extracting the vertical loading profile.

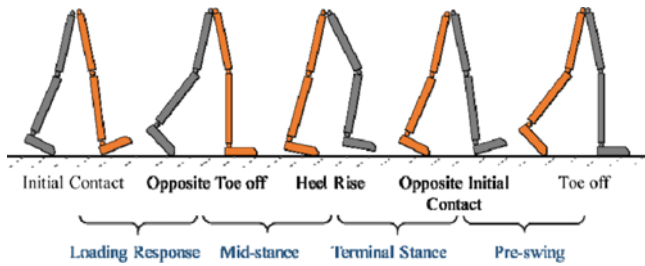During the stance phase, the ground reaction force (GRF) is exerted

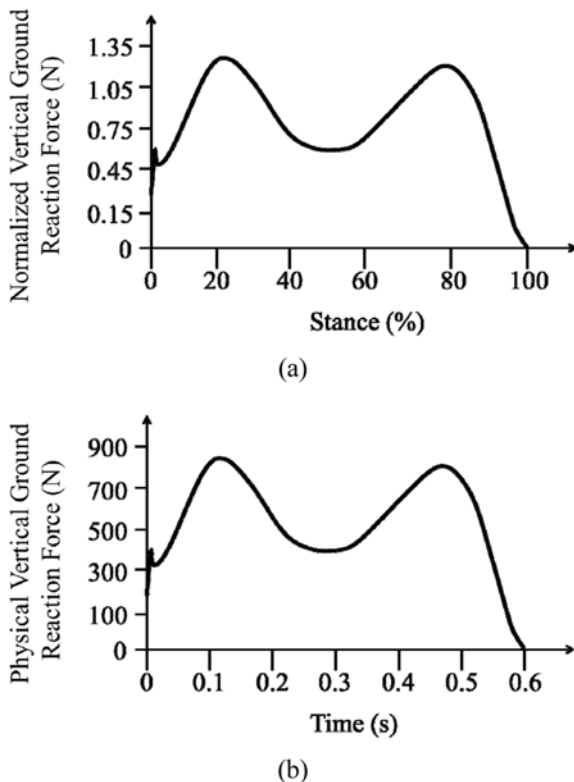Fig. 1 Stance phase of the gait cycle under human walking



Fig. 3 Configuration of the OBEH sidewalk (top view)



(a)



(b)

Fig. 2 Vertical component of the ground reaction force (VGRF) profile: (a) normalized VGRF[18] and (b) physical VGRF

by the ground on the human's foot in contact with it. This GRF provides the transient vertical loading profile, which includes the magnitude and direction of the force along the center of pressure (COP) path beneath the foot. The GRF vector represents the sum of all forces acting between the sole of the foot and its supporting surface. The GRF vector can be decomposed into the vertical, mediolateral, and anteroposterior components. The vertical component of the GRF (VGRF) is the most dominant force causing deflection of the OBEH sidewalk block.

Fig. 2(a) shows the normalized VGRF, which was experimentally observed by Hunt et al..[18] The normalized VGRF forms a double hump (two distinctive maxima) of which magnitudes are greater than 1 N. The normalized VGRF of 1 N corresponds to body weight. The initial small peak is produced by a heel strike. The first hump is associated with an upward acceleration of the COP path during early stance, while the second hump results from a deceleration due to the downward
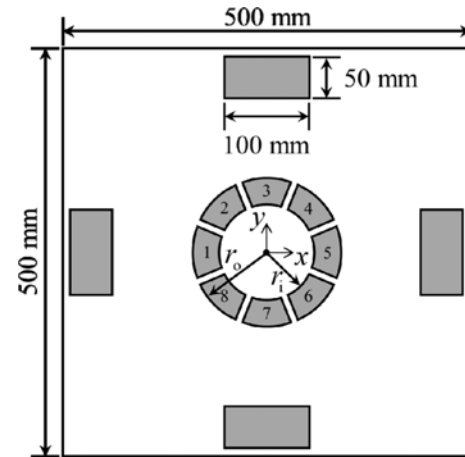
motion in the late stance.[19]

In this study, the normalized VGRF is converted to the physical VGRF by multiplying the average weight of 70 kg for Korean adult males, as shown in Fig. 2(b). In addition, the average speed and stride of human walking are about 1 m/s and 1 m, respectively, and the stance phase accounts for 60% of one gait cycle. Therefore, the duration time of the stance phase from 'initial contact' to 'toe off' is assumed to be 0.6 seconds. In this study, the physical VGRF in Fig. 2(b) will be used as the vertical loading profile in the transient analysis of the OBEH sidewalk block outlined in Section 3.

## 2.2 Configuration of the Omnidirectional Biomechanical Energy Harvesting Sidewalk Block

Since pedestrians walk along in arbitrary directions, it is of great importance to produce the desired output energy regardless of the direction and position of the footsteps. To properly deal with the randomness in the footsteps, this study newly proposes the concept of an omnidirectional biomechanical energy harvesting (OBEH) sidewalk block. As shown in , the piezoelectric layers are deployed in an annulus shape at the center on the 'top surface' of the structural layer in a unimorph configuration. A three-dimensional Cartesian coordinate system $(x, y, z)$ is established, as shown in Fig. 3. The origin $(0, 0, 0)$ of the coordinate system is located at the center on the bottom surface of the structural layer and the $z$-axis is toward the top surface. The OBEH sidewalk block is doubly symmetric with respect to the $x$-$y$ plane. Pedestrians directly step on the 'bottom surface' of the structural layer.

The annular piezoelectric layers are divided into eight segments due to the maximum allowable size. There is no particular rule in segmenting the annular piezoelectric layers attached on the center of the structural layer, as long as the manufacturability is ensured. Comparison of Figs. 1 and 2 clearly suggests that the OBEH sidewalk block may undergo large deflections at the instants during the 'loading response' and the 'pre-swing', respectively. The annular deployment of the piezoelectric layers attached to the center of the structural layer can effectively cover the regions with which the human's foot is in contact at the instants corresponding to the double hump of the physical VGRF, for any direction. The four rectangular piezoelectric layers are attached

near the edges. All the piezoelectric layers operate in a 31-mode, in which the direction of the applied mechanical stress and that of the output voltage are perpendicular to each other. Since the mechanical strain induced on the corners of the structural layer with the fully clamped boundary condition is very small, it is not necessary to allocate the piezoelectric layers on the corners.

The boundary condition of the structural layer is fully clamped (CCCC). This implies that the applied strains in the four rectangular piezoelectric layers attached near the edges of the structural layer have the opposite sign of those of the annular piezoelectric layers attached to the center, when a pedestrian steps on the top surface of the structural layer. Since the output voltage generated by the piezoelectric layer is proportional to the applied strain, the tensile strain yields a positive output voltage, and vice versa.[20,21] Therefore, the output voltage could decrease significantly when there is a sign change (i.e., inflection lines) of the applied strain in the piezoelectric layer.[6] This electroelastic phenomenon is called voltage cancellation, which leads to important design-related rationales for selecting optimal placement of the piezoelectric layers.[22,23] That is why the annular and rectangular piezoelectric layers are attached to the center of the structural layer and near the edges, respectively.

The dimensions of the length and width of the OBEH sidewalk block were determined in accordance with the average foot size; both are 500 mm. The thickness of all the piezoelectric layers ($h_p$) is 0.2667 mm. The length and width of the rectangular piezoelectric layers are 100 mm and 50 mm, respectively. It should be noted that the thickness of the structural layer ($h_s$), inner radius ($r_i$) and outer radius ($r_o$) of the annular piezoelectric layers will be treated as design variables in Section 4. In this study, all the piezoelectric layers are made of PZT-5H4E, which has a high electroelastic coupling. The structural layer is made of stainless steel for high corrosion resistance. Of course, various combinations of materials are acceptable to serve a particular design purpose.

## 3. Electroelastically Coupled Finite Element Modeling of the Omnidirectional Biomechanical Energy Harvesting Sidewalk Block

This section describes the investigations of the transient output performances of the OBEH sidewalk block when it undergoes a mechanical bending stress subject to the vertical loading profile extracted from human gait analysis. It has been reported throughout the published literature[24,25] that a finite element (FE) model for piezoelectric energy harvesting have high predictive capability. In this study, therefore, the electroelastically coupled FE model of the OBEH sidewalk block was implemented using ANSYS® Workbench™ R17.0. Section 3.1 explains the procedure of the FE modeling and Section 3.2 describes the transient output responses of the OBEH sidewalk block under the vertical loading profile

### 3.1 Procedure of Finite Element Modeling

According to the IEEE Standard on linear piezoelectricity,[26] the constitutive relations of the piezoelectric layers are given in a stress-charge form as:

Table 1 Material properties of the piezoelectric and structural layers

| Description | | Nominal value |
|---|---|---|
| Structural layer (Stainless steel) | Young's modulus | 200 GPa |
| | Poisson's ratio | 0.31 |
| | Density | 7750 Kg/m$^3$ |
| Piezoelectric layer (PZT-5H4E) | Elastic compliance — $s_{11}$ | 16.50 pm$^2$/N |
| | $s_{12}$ | -4.78 pm$^2$/N |
| | $s_{13}$ | -8.45 pm$^2$/N |
| | $s_{33}$ | 20.70 pm$^2$/N |
| | $s_{44}$ | 43.50 pm$^2$/N |
| | $s_{66}$ | 42.60 pm$^2$/N |
| | Density | 7500 Kg/m$^3$ |
| | Piezoelectric strain coefficient | -274 pm/V |
| | Piezoelectric constant | -6.62 C/m$^2$ |
| | Dielectric permittivity at constant strain | 17.29 nF/m |

$$T_{ij} = c_{ijkl}S_{kl} - e_{kij}E_k \tag{1}$$

$$D_i = e_{ikl}S_{kl} + \varepsilon_{ij}E_j \tag{2}$$

where $c_{ijkl}$, $T_{ij}$, and $S_{kl}$ denote the elastic modulus, the stress, and the strain, respectively, in the mechanical domain. In the electrical domain, $D_i$, $\varepsilon_{ij}$, and $E_j$ denote the electric displacement, the dielectric permittivity, and the electric field, respectively. Please note that Eqs. (1) and (2) are coupled by the piezoelectric constant $e_{kij}$.

The structural layer was modeled by a SOLID186 element possessing three translational degrees of freedom (DOFs). The piezoelectric layers were modeled by a SOLID226 element having four coupled-field DOFs (three translational displacements and one electric potential). It was assumed that the electrode layer and the adhesive material are negligible. In the SOLID226 element, the VOLT DOF was used to couple the output voltage on the upper surface of the piezoelectric layer, thereby representing the top electrode. The interface between the piezoelectric layer and the structural layer was grounded (zero electric potential) to represent the bottom electrode. The top and bottom electrodes were connected with an external electrical resistance using a CIRCU94 element that was employed for piezoelectric-circuit analysis. Since the piezoelectric layers are assumed to be poled along the z-axis, the electric field was applied in the z-direction only.

Steady-state excitation is not commonly available in human walking. Instead, the profile of the VGRF on the footstep was applied to the selected positions as nodal forces in transient analysis. The selected positions for nodal forces forms in a shape of a sole. The profile of the VGRF in Fig. 2(b) belonging to the stance phase was divided into 17 steps. The VGRF of each step was applied as the nodal force on the selected position.

The nominal values of the material properties of the piezoelectric and structural layers are summarized in Table 1. In this study, the term 'nominal' implies the existence of inherent variability in the material properties. Please note that the geometry of the OBEH sidewalk block considered in Section 3 is the initial design. Numerical damping, which is associated with the time-stepping schemes used for integrating second-order systems of equations over time, was set to 0.1 in transient analysis.
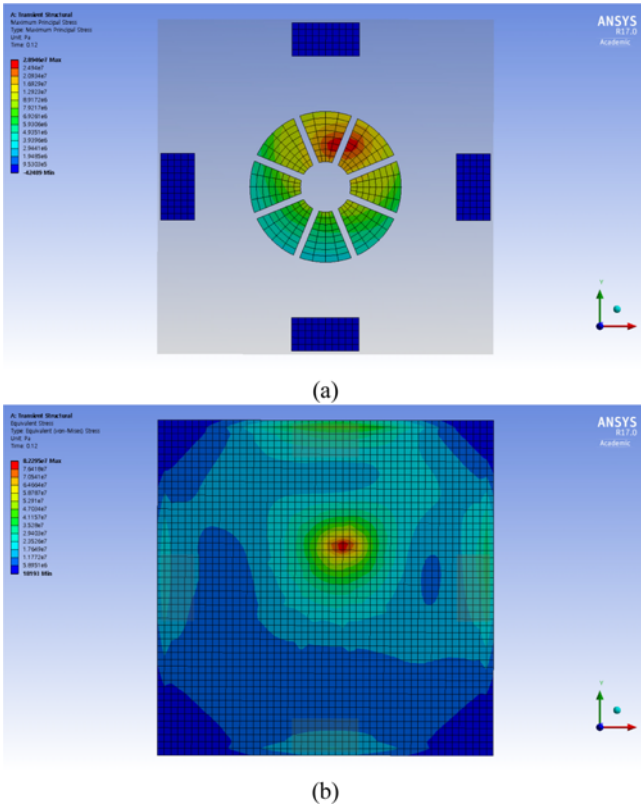
(a)



(b)

Fig. 4 Transient structural analysis of the OBEH sidewalk block under straight walking along the negative $y$-axis at 0.12 seconds: (a) maximum principal stress of the piezoelectric layers and (b) von-Mises stress of the structural layer



(a)



(b)

Fig. 5 Time-variant output voltage across various external electrical resistances generated by: (a) the 3rd segment and (b) the 7th segment

## 3.2 Output Responses of the Omnidirectional Biomechanical Energy Harvesting Sidewalk Block

### 3.2.1 Mechanical Bending Stress

The OBEH sidewalk block is initially at rest (null stress and output voltage). When a pedestrian steps on the OBEH sidewalk block, the piezoelectric and structural layers undergo a mechanical bending stress. Repeatedly applied mechanical bending stress can lead to accumulation of microscopic damage, thereby giving rise to fatigue failure of the OBEH sidewalk block. Since the structural layer is made of the ductile material (stainless steel), its fatigue life is controlled by the octahedral shear stress (von-Mises stress) criterion under a state of multiaxial stress. On the other hand, since the piezoelectric layers (PZT-5H4E) are brittle, the maximum principal stress is a concern.

As shown in Fig. 2(b), the magnitude of the VGRF between the 'initial contact' and the 'opposite toe off' during the stance phase reaches its maximum at 0.12 s. This implies that the deflection of the OBEH sidewalk block is expected to be its maximum at this moment. For the initial design of the OBEH sidewalk block, Figs. 4(a) and 4(b) depict the maximum principal stress of the piezoelectric layer and the von-Mises stress of structural layer at 0.12 s, respectively. Fig. 4(a) clearly manifests the effectiveness of the deployment of the annular piezoelectric layers attached to the center of the structural layer, because the area covers enough of the large strains. The desired level of reliability with respect to the maximum principal stress of the
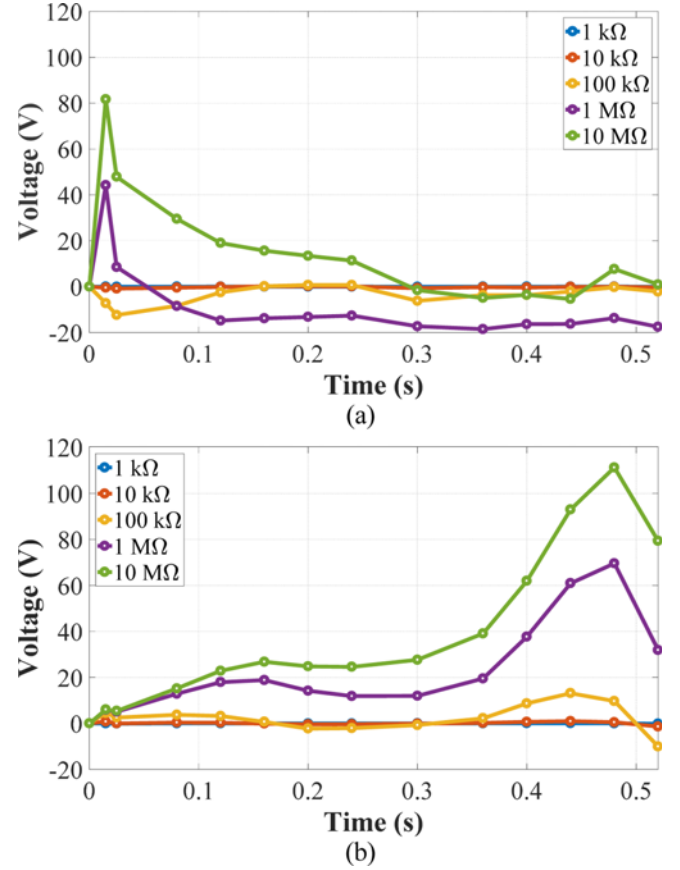
piezoelectric layers is considered as the probabilistic constraint in the procedure of reliability-based design optimization (RBDO) of the OBEH sidewalk block. This will be explained in Section 4.

### 3.2.2 Output Electrical Performances

The conversion of biomechanical energy into electricity during human walking is the most important function of the OBEH sidewalk block. Since a piezoelectric layer possesses its own capacitance, it can be described as an equivalent resistance-capacitor (RC) circuit. It is well known that the output electrical performances (i.e., the output voltage) of the equivalent RC circuit are affected by a time constant $\tau$. $\tau$ is the time required to charge the capacitor and is expressed as:

$$\tau = R_{\mathrm{L}} C_{\mathrm{p}} \tag{3}$$

where $R_{\mathrm{L}}$ and $C_{\mathrm{p}}$ denote the external electrical resistance and the capacitance, respectively. The capacitance can be calculated by:

$$C_{\mathrm{p}} = \frac{\varepsilon_{33}^{S} A_{\mathrm{p}}}{h_{\mathrm{p}}} \tag{4}$$

where $\varepsilon_{33}^{s}$ denotes the dielectric permittivity at constant strain. $A_{\mathrm{p}}$ denotes the top surface area of one piezoelectric layer. This study assumed that all segments deploying the annular shape have the same dimensions. In Eq. (4), since the dielectric permittivity at constant
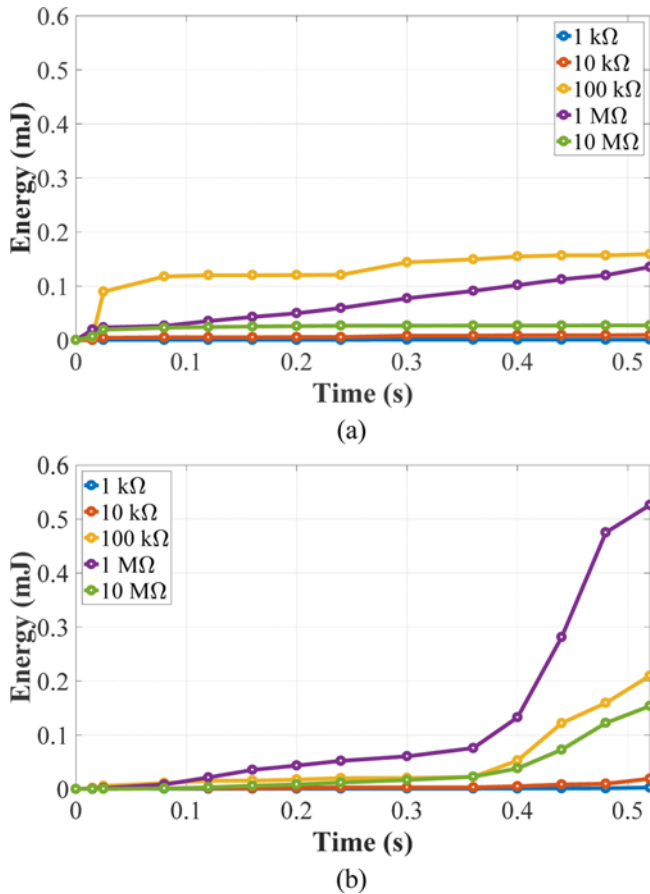
Fig. 6 Output energy across various external electrical resistances generated by: (a) the 3rd segment and (b) the 7th segment

strain and the thickness of the piezoelectric layer are constant values, the nominal value of the capacitance varies only with the top surface area of the piezoelectric layer. This implies that the time constant is determined by the top surface area of the piezoelectric layer and the external electrical resistance.

Unlike harmonic analysis, the time constant is a critical parameter in transient analysis of the OBEH sidewalk block under human walking. Fig. 5 shows the time-variant output voltage across various external electrical resistances generated by the 3rd and 7th segments of the annular piezoelectric layers. During the 'loading response' of the footstep, the 3rd segment produces the high output voltage in a moment during early stance, as shown in Fig. 5(a). Likewise, during the 'pre-swing' of the footstep, the 7th segment produces the high output voltage in a moment during early stance, as shown in Fig. 5(b).

For low values of the external electrical resistance (i.e., 1 kΩ and 10 kΩ), the time-variant output voltage generated by the 3rd segment decays to zero rapidly, since the time constant is small. This is because the time constant of the equivalent RC circuit leads to the electrical damping effect under the transient footstep loading. As the external electrical resistance increases, the time constant gets larger, and thereby the time-variant output voltage decays slowly. For instance, the form of the time-variant output voltage almost resembles that of the VGRF profile when the external electrical resistance is 10 MΩ. In this study, an external electrical resistance of 10 MΩ was considered as the open circuit condition (the time constant approaches infinity). When the

magnitude of the external electrical resistance was small, negative values of the time-variant output voltage were observed, because the capacitor of the piezoelectric layer begins to discharge over time. Therefore, an energy quantity (in the duration of the stance phase), rather than the output electric power (at a certain moment), was considered as the objective function to be maximized in design optimization of the OBEH sidewalk block, as described in Section 4.

Fig. 6 shows the output energy across various external electrical resistances generated by the 3rd and 7th segments of the annular piezoelectric layers. Since the output energy varies with the external electrical resistance, the optimal value to maximize the output energy should be determined in the process of design optimization. When the external electrical resistance is set to its optimal value, the maximum output electric power can be achieved; this is called impedance matching. In this study, therefore, the external electrical resistance was considered as one of the design variables in the RBDO of the OBEH sidewalk block.

## 4. Design Optimization of the Omnidirectional Biomechanical Energy Harvesting Sidewalk Block under Uncertainty

This section explains the design optimization process of the OBEH sidewalk block. Since deterministic design optimization does not consider physical uncertainty in the material properties and manufacturing tolerance, it may result in unreliable solutions.[27] Furthermore, the position and direction of the footstep during human walking are inherently random as well. In the design process, it is thus of critical importance to analyze uncertainty propagation by which the variability of the input variables is propagated to the variation in the output performances.[28] In this study, therefore, the RBDO was executed so that the output energy of the OBEH sidewalk block was reliably generated, while accounting for physical uncertainty in not only the material properties and the manufacturing tolerance but also uncertainty in the footstep during human walking. Section 4.1 describes the formulations for design optimization of the OBEH sidewalk block. Section 4.2 explains the design and noise variables. Section 4.3 explains the optimization algorithms; a response surface methodology (RSM) with design of experiment (DOE) is described in Section 4.4. The design optimization results are provided in Section 4.5.

### 4.1 Design Formulation
The design optimization procedure of the OBEH sidewalk block consists of two sequentially-executed processes. First, deterministic design optimization (DDO) was applied to maximize the output energy (the objective function), while satisfying the high-cycle fatigue (HCF) failure constraints. The RBDO was then sequentially launched starting at the DDO solution. In the RBDO, the HCF was incorporated into the probabilistic constraint of design optimization of the OBEH sidewalk block. Since the HCF is relevant to the stress-based approach, the maximum bending stress was considered as a fatigue failure constraint in design of the reliable OBEH sidewalk block.

The DDO of the OBEH sidewalk block can be formulated as:

$$\text{Maximize} \sum_{i=1}^{np} OE_i(\mathbf{d})$$

$$\text{Subject to } G(\mathbf{d}) < 0 \tag{5}$$

$$\mathbf{d_L} \leq \mathbf{d} \leq \mathbf{d_U}, \ \mathbf{d} \in R^{nd}$$

$$\text{where } G(\mathbf{d}) = \sigma(\mathbf{d}) - \overline{\sigma}_e$$

where OE denotes the output energy with np being the number of the annular piezoelectric layers ($np = 8$); $\mathbf{d}$ denotes the design vector. $G(\mathbf{d})$ denotes the performance function against fatigue failure of the piezoelectric layers, where $\sigma$ and $\overline{\sigma}_e$ are the maximum principal stress of the piezoelectric layer and the nominal value of the fatigue limit, respectively. In this study, the mean value of the fatigue limit of the piezoelectric layers was assumed to be 48.3 MPa[29] and the coefficient of variance (COV) was assumed to be 0.2. The superscript nd denotes the number of design variables ($nd = 4$). In this study, the output energy is indicated by the sum of the output energy generated by eight center piezoelectric layers. $\mathbf{d_L}$ and $\mathbf{d_U}$ are the lower and upper bounds of the design variables, respectively.

The RBDO problem of the OBEH sidewalk block was formulated as:

$$\text{Maximize} \sum_{i=1}^{np} OE_i(\mathbf{d})$$

$$\text{Subject to } P[G(\{\mathbf{X};\mathbf{d(X)}\} < 0)] > P_t \tag{6}$$

$$\mathbf{d_L} \leq \mathbf{d} \leq \mathbf{d_U}, \ \mathbf{d} \in R^{nd} \text{ and } \mathbf{X} \in R^{nr}$$

$$\text{where } G\{\mathbf{X};\mathbf{d(X)}\} = \sigma\{\mathbf{X};\mathbf{d(X)}\} - \sigma_e$$

where $\mathbf{X}$ denotes the random vector with the superscript nr being the number of random noise variables ($nr = 6$). Through the RBDO, the output energy is maximized while satisfying the probabilistic constraint of fatigue failure of the piezoelectric layer. It is worth pointing out that the fatigue limit $\sigma_e$ in Eq. (6) is assumed to follow a normal distribution, while the fatigue limit $\overline{\sigma}_e$ in Eq. (5) is a nominal value. The probabilistic constraints are described by the performance function $G\{\mathbf{X};\mathbf{d(X)}\}$ and the target reliability $P_t$ is defined as 99.87%.

### 4.2 Definition of Design and Noise Variables

This study considers four design variables including: the inner radius and the outer radius of the annular piezoelectric layers, denoted by $r_i$ and $r_o$, respectively; the thickness of the structural layer, denoted by $h_s$; and the external electrical resistance of the annular piezoelectric layers, denoted by $R_L$. The external electrical resistance of the annular piezoelectric layers was considered as a deterministic design variable, while the other three design variables were assumed to follow a normal distribution due to variability in the geometry. The output energy generated by the four rectangular piezoelectric layers attached near the edges is much lower than that by the eight annular piezoelectric layers attached to the center of the structural layer. In addition, the design change of the rectangular piezoelectric layers has little influence on the output energy and maximum principal stress of the annular piezoelectric layers. This is why this study only considers the design variables related to the annular piezoelectric layers. After completing design optimization of the annular piezoelectric layers, the similar approach can be applied sequentially to the rectangular piezoelectric layers.

Table 2 Information about the design variables

| Design variables | | Statistical information | | | Design bounds | |
|---|---|---|---|---|---|---|
| Notation | Unit | Type | Distribution | Mean | Lower | Upper |
| $r_i$ | mm | Random | Normal | 37.5 | 25.0 | 50.0 |
| $r_o$ | mm | Random | Normal | 112.5 | 100.0 | 125.0 |
| $h_s$ | mm | Random | Normal | 4.0 | 1.0 | 7.0 |
| $R_L$ | kΩ | Deterministic | | 300 | 100 | 500 |

The upper and lower bounds of the design variables should be carefully decided based on the scientific rationales. If the inner radius reaches the upper bound and outer radius is determined as the lower bound, the top surface area of the annular piezoelectric layers becomes the minimum. The upper bound of the inner radius and the lower bound of the outer radius were decided to allow the minimum area covered with the annular piezoelectric layers to contain at least the region where the high strains occur. In addition, the maximum size of the top surface of the annular piezoelectric layers should be smaller than the practically producible dimension of PZT-5H4E (i.e., 100 mm). Therefore, the lower bound of the inner radius and the upper bound of the outer radius were decided to take into account the manufacturability of the annular piezoelectric layers. The design bounds of the external electrical resistance were decided based on the preliminary results that the maximum output energy was expected to be achieved in the range of 100 kΩ to 500 kΩ, as shown in . In order to have a large enough feasible region for the RBDO, the design bounds of the thickness of the structural layer were defined from 2 mm to 5 mm. The details of the design variables are summarized in Table 2.

To characterize variability in the material properties, three noise variables were considered including the Young's modulus of the structural layer, the elastic compliance of the piezoelectric layer, $s_{11}$, and the piezoelectric strain coefficient of the piezoelectric layer, $d_{31}$. To consider the randomness of the footstep, three noise variables were considered, including the position of the footstep with respect to the x- and y-axes, and the angle of the footstep. The COV of the material properties and geometry are 0.05 and 0.01, respectively. The mean values can be found in Table 1. The statistical information of the footstep during human walking is summarized in Table 3.

### 4.3 Optimization Algorithms

The double-loop RBDO algorithm was implemented in this study, which includes reliability analysis (inner loop) and structural optimization (outer loop). In the inner loop, reliability was calculated by the Monte Carlo simulation (MCS) as:

$$P[G\{\mathbf{X};\mathbf{d(X)}\} < 0] \cong \frac{1}{ns} \sum_{r=1}^{ns} I_{\Omega_{safe}}[\mathbf{x}_r] \tag{7}$$

where ns is the number of runs for the MCS and $\Omega_{safe}$ denotes the safe domain. In this study, the number of runs for the MCS was 100,000. $I[\bullet]$ denotes the indicator function of a "safe" or "fail" domain, such that:

$$I_{\Omega_{safe}}[\mathbf{x}_r] = \begin{cases} 1, \mathbf{x}_r \in \Omega_{safe} \\ 0, \mathbf{x}_r \notin \Omega_{safe} \end{cases} \tag{8}$$

Table 3 Statistical information of the footstep

| Description | Distribution | Parameters | |
|---|---|---|---|
| | | Minimum | Maximum |
| Footstep position (x-axis) | Uniform | -100 mm | 100 mm |
| Footstep position (y-axis) | Uniform | -100 mm | 100 mm |
| Footstep direction (angle) | Uniform | 0 | $\pi$ |

In the outer loop, the evolutionary algorithm (EA) was implemented using a commercially-available software, PIAnO (Process Integration, Automation and Optimization) 2014, to find an optimal design for maximizing the output energy generated by the OBEH sidewalk block. The EA was based on the collective learning process within a population of individuals; it mimics the mechanics of natural selection and genetics.[30,31] The EA was also used to solve the DDO.

## 4.4 Response Surface Methodology (RSM) with Design of Experiment (DOE)

Since the MCS requires a large number of function evaluations to achieve satisfactory accuracy of reliability analysis, this study implemented the response surface methodology (RSM) to alleviate the computational burden of the electroelastically coupled FE model of the OBEH sidewalk block. The RSM is a collection of statistical and mathematical techniques useful for developing, improving, and optimizing processes.[32-34] Once the accurate RSM is available, the RBDO can be executed in a cost-effective manner. A systematic method for gathering the response data is required to implement the RSM in the design space.[35] Two primary procedures are involved with collecting the response data: (1) design of experiment (DOE) and (2) surrogate modeling (or response approximation).

In this study, a Latin Hypercube sampling (LHS) method was used to perform the DOE. The LHS method is a space-filling technique with good uniformity and flexibility to generate training points, whereby only one training point is located in each axis-aligned hyperplane. The bounds of the DOE for the random design and noise variables are defined by the target reliability of 99.87%. For instance, the minimum and maximum values of the DOE for the random design variables are defined as $\mathbf{d}_L-3\sigma_d$ and $\mathbf{d}_U+3\sigma_d$, respectively, where $\sigma_d$ denotes the standard deviation vector of the random design variables. The lower and upper bounds of the DOE for the random noise variables correspond to $\mu_X-3\sigma_X$ and $\mu_X+3\sigma_X$, respectively, where $\sigma_X$ denotes the standard deviation vector of the random noise variables.

The number of the training points nt necessary to construct the RSM[36] is determined as:

$$nt = \frac{q(nd+nr+1)(nd+nr+2)}{2} \qquad (9)$$

where $q$ can be settled based on the scale (scarce, small, and large) of a problem. In this study, the total number of the design and noise variables was 10 ($nd = 4$ and $nr = 6$). By setting $q$ to 3.5, 231 training points were generated by the LHS method to construct a reasonably accurate RSM.

The normalized root mean square error (NRMSE) and the R-squared were used to evaluate the accuracy of the surrogate model candidates.[36,37] 30 testing points were additionally generated by the LHS design method. It can be concluded from the testing results that

Table 4 Final selection of surrogate models

| | Maximum principal stress of piezoelectric layers | von-Mises stress of structural layer | Output energy |
|---|---|---|---|
| Basis function | Polynomial (simple cubic) | Polynomial (simple cubic) | Kriging (linear) |
| NRMSE | 0.075 | 0.080 | 0.120 |
| R-Square | 0.821 | 0.908 | 0.885 |

Table 5 Design optimization results of the OBEH sidewalk block

| Category | | Initial | DDO | RBDO |
|---|---|---|---|---|
| Design variables (mean) | Inner radius of piezoelectric layers | 37.5 mm | 25.81 mm | 25.15 mm |
| | Outer radius of piezoelectric layers | 112.50 mm | 115.95 mm | 124.99 mm |
| | Thickness of structural layer | 4.00 mm | 3.18 mm | 3.50 mm |
| | External electrical resistance | 400.00 kΩ | 274.78 kΩ | 200.47 kΩ |
| Output energy (mean) | FEM | 5.12 mJ | 13.69 mJ | 9.97 mJ |
| | RSM | 4.69 mJ | 12.80 mJ | 10.14 mJ |
| | Percentage difference | 8.46 % | 6.50 % | 1.70 % |
| Maximum principal stress (mean) | FEM | 33.39 MPa | 51.11 MPa | 41.40 MPa |
| | RSM | 34.96 MPa | 48.64 MPa | 41.24 MPa |
| | Percentage difference | -4.73 % | 4.83 % | 0.40 % |
| Reliability | | 100.00 % | 74.86 % | 99.79 % |

the simple cubic polynomial is acceptable as a surrogate model for both the maximum principal stress of the piezoelectric layers and the maximum von-Mises stress of the structural layer. Table 4 summarizes the final selection of the surrogate models. Details about the RSM with the DOE can be found in the published literatures.[32,36,37]

## 4.5 Results and Discussion

The design optimization results are summarized in Table 5. The output energy generated by the OBEH sidewalk block was 12.80 mJ (RSM) in the DDO case, and 10.14 mJ (RSM) in the RBDO case. In the DDO case, the maximum output electric power of 21.69 mW was achieved at 0.48 s by the 7th segment across the external electrical resistance of 274.78 kΩ. In the RBDO case, the maximum output electric power of 18.52 mW was achieved at 0.48 s by the 7th segment across the external electrical resistance of 200.47 kΩ. It is worth pointing out that the DDO violates the probabilistic mechanical durability constraint, even though it can achieve higher output energy than the RBDO. Since the RBDO maximizes the output energy while satisfying the target reliability of the stress constraints, reliability substantially increases from 74.86% (DDO) to 99.79% (RBDO). In addition, even though reliability for the RBDO is almost the same as that for the initial design, the former can achieve the much higher output energy than the latter (almost two times). It can be thus concluded that probabilistic optimum design of the OBEH sidewalk block is a practical solution to reliably generate the output energy while achieving the target reliability regardless of uncertainty sources.

As shown in Table 5, the thickness of the structural layer for the RBDO (3.50 mm) is larger than that for the DDO (3.18 mm). The design change from the DDO to the RBDO means becoming more conservative. The more conservative design in terms of the thickness of the structural layer sacrifices the amount of the mechanical strain, thereby slightly sacrificing the output energy. This is because the higher absolute value of the in-plane normal strains ensures larger voltage generation. However, as the structural layer gets thicker, the maximum principal stress of the piezoelectric layers decreases, thereby enhancing reliability of fatigue failure.

In addition, for both the DDO and the RBDO, the inner radius of the annular piezoelectric layers is decreased compared to the initial design, while the outer radius is increased. This implies that the sizes of the top surface of the annular piezoelectric layers are increased to effectively cover the regions at which the high mechanical strains occur. A parametric study showed that there was no apparent tendency of the outer radius $r_o$ on the maximum principal stress of the annular piezoelectric layers, compared to the inner radius $r_i$. This could be the reason why the outer radius $r_o$ gets very close to its upper bound to maximize the output energy.

## 5. Conclusions

This study proposed an omnidirectional biomechanical energy harvesting (OBEH) sidewalk block that generates electricity from human walking during daily activities. The eight piezoelectric layers are deployed in an annulus shape at the center of the bottom surface of the structural layer in a unimorph configuration. The annular deployment of the piezoelectric layers attached to the center of the structural layer has the advantage of being able to effectively cover the areas at which high strains occur. The four rectangular piezoelectric layers are attached near the edges. The design framework of the proposed OBEH sidewalk block consists of three sequentially-executed steps: (1) extraction of a footstep loading profile from human gait analysis; (2) electroelastically coupled FE modeling to estimate the transient output responses under the footstep loading profile; and (3) the RBDO of the OBEH sidewalk block under physical uncertainty, including inherent variability in the material properties and geometry (device uncertainty) and the randomness in the position and direction of the footstep (loading uncertainty).

Since steady-state excitation is not as commonly available in human walking, the profile of the VGRF on the footstep was applied as the loading condition in the transient analysis. Unlike harmonic analysis, the time constant plays a critical role in analyzing the electroelastic behaviors of the OBEH sidewalk block under transient human walking. As the external electrical resistance increases, the time constant gets larger, and thereby the time-variant output voltage decays slowly. When the magnitude of the external electrical resistance is small, negative values of the time-variant output voltage are observed. This is because the capacitor of the piezoelectric layer begins to discharge over time. The RBDO problem was formulated to maximize the output energy generated by the annular piezoelectric layers attached to the center of the structural layer, while achieving the target reliability of 99.87%. The design variables for size change included the inner radius and the outer radius of the annular piezoelectric layers, as well as the

thickness of the structural layer. Since there exists the optimal value of the external electrical resistance to maximize the output energy, the external electrical resistance of the annular piezoelectric layers was also considered as a design variable in design optimization. It can be concluded from the results that the proposed OBEH sidewalk block enables useful power generation while satisfying the target reliability of fatigue failure under uncertainty.

Since all of the four edges of the structural layer are fully clamped, the OBEH sidewalk block may undergo geometric nonlinearity when relatively large forces. Therefore, the effects of geometric nonlinearity on the output energy of the OBEH sidewalk block will be included in the future work.

## ACKNOWLEDGEMENT

## DECLARATION OF CONFLICTING INTERESTS

The author(s) declared no potential conflicts of interest with respect to the research, authorship, and/or publication of this article.

## REFERENCES

1. Kim, H. S., Kim, J.-H., and Kim, J., "A Review of Piezoelectric Energy Harvesting Based on Vibration," International Journal of Precision Engineering and Manufacturing, Vol. 12, No. 6, pp. 1129-1141, 2011.

2. Kim, J. E., Kim, H., Yoon, H., Kim, Y. Y., and Youn, B. D., "An Energy Conversion Model for Cantilevered Piezoelectric Vibration Energy Harvesters Using Only Measurable Parameters," International Journal of Precision Engineering and Manufacturing-Green Technology, Vol. 2, No. 1, pp. 51-57, 2015.

3. Park, H. and Kim, J., "Electromagnetic Induction Energy Harvester for High-Speed Railroad Applications," International Journal of Precision Engineering and Manufacturing-Green Technology, Vol. 3, No. 1, pp. 41-48, 2016.

4. Park, J.-H., Lim, T.-W., Kim, S.-D., and Park, S.-H., "Design and Experimental Verification of Flexible Plate-Type Piezoelectric Vibrator for Energy Harvesting System," International Journal of Precision Engineering and Manufacturing-Green Technology, Vol. 3, No. 3, pp. 253-259, 2016.

5. Park, H., "Vibratory Electromagnetic Induction Energy Harvester on Wheel Surface of Mobile Sources," International Journal of Precision Engineering and Manufacturing-Green Technology, Vol. 4, No. 1, pp. 59-66, 2017.

6. Yoon, H., Youn, B. D., and Kim, H. S., "Kirchhoff Plate Theory-Based Electromechanically-Coupled Analytical Model Considering Inertia and Stiffness Effects of a Surface-Bonded Piezoelectric Patch," Smart Materials and Structures, Vol. 25, No. 2, Paper No. 025017, 2016.

7. Erturk, A. and Inman, D. J., "On Mechanical Modeling of Cantilevered Piezoelectric Vibration Energy Harvesters," Journal of Intelligent Material Systems and Structures, Vol. 19, No. 11, pp. 1311-1325, 2008.

8. Erturk, A. and Inman, D. J., "An Experimentally Validated Bimorph Cantilever Model for Piezoelectric Energy Harvesting from Base Excitations," Smart Materials and Structures, Vol. 18, No. 2, Paper No. 025009, 2009.

9. Usharani, R., Uma, G., and Umapathy, M., "Design of High Output Broadband Piezoelectric Energy Harvester with Double Tapered Cavity Beam," International Journal of Precision Engineering and Manufacturing-Green Technology, Vol. 3, No. 4, pp. 343-351, 2016.

10. Yun, S.-M. and Kim, C., "The Vibrating Piezoelectric Cantilevered Generator under Vortex Shedding Excitation and Voltage Tests," International Journal of Precision Engineering and Manufacturing, Vol. 17, No. 12, pp. 1615-1622, 2016.

11. Aggarwal, J. K. and Cai, Q., "Human Motion Analysis: A Review," Computer Vision and Image Understanding, Vol. 73, No. 3, pp. 428-440, 1999.

12. Simon, S. R., "Quantification of Human Motion: Gait Analysis-Benefits and Limitations to Its Application to Clinical Problems," Journal of Biomechanics, Vol. 37, No. 12, pp. 1869-1880, 2004.

13. Riemer, R. and Shapiro, A., "Biomechanical Energy Harvesting from Human Motion: Theory, State of the Art, Design Guidelines, and Future Directions," Journal of Neuroengineering and Rehabilitation, Vol. 8, No. 1, DOI: 10.1186/1743-0003-8-22, 2011.

14. Shenck, N. S. and Paradiso, J. A., "Energy Scavenging with Shoe-Mounted Piezoelectrics," IEEE Micro, Vol. 21, No. 3, pp. 30-42, 2001.

15. Zhao, J. and You, Z., "A Shoe-Embedded Piezoelectric Energy Harvester for Wearable Sensors," Sensors, Vol. 14, No. 7, pp. 12497-12510, 2014.

16. Pozzi, M. and Zhu, M., "Plucked Piezoelectric Bimorphs for Knee-Joint Energy Harvesting: Modelling and Experimental Validation," Smart Materials and Structures, Vol. 20, No. 5, Paper No. 055007, 2011.

17. Ko, C.-Y., Ko, J., Kim, H. J., and Lim, D., "New Wearable Exoskeleton for Gait Rehabilitation Assistance Integrated with Mobility System," International Journal of Precision Engineering and Manufacturing, Vol. 17, No. 7, pp. 957-964, 2016.

18. Hunt, A. E., Smith, R. M., Torode, M., and Keenan, A.-M., "Inter-Segment Foot Motion and Ground Reaction Forces Over the Stance Phase of Walking," Clinical Biomechanics, Vol. 16, No. 7, pp. 592-600, 2001.

19. Levine, D., Richards, J., and Whittle, M., "Whittle's Gait Analysis," Churchill Livingstone/Elsevier, 5th Ed., 2012.

20. Yoon, H. and Youn, B. D., "Stochastic Quantification of the Electric Power Generated by a Piezoelectric Energy Harvester Using a Time-Frequency Analysis under Non-Stationary Random Vibrations," Smart Materials and Structures, Vol. 23, No. 4, Paper No. 045035, 2014.

21. Yoon, H., Kim, M., Park, C.-S., and Youn, B. D., "Time-Varying Output Performances of Piezoelectric Vibration Energy Harvesting under Nonstationary Random Vibrations," Smart Material Structures, Vol. 27, No. 1, Paper No. 015004, 2018.

22. Lee, S. and Youn, B. D., "A New Piezoelectric Energy Harvesting Design Concept: Multimodal Energy Harvesting Skin," IEEE Transactions on Ultrasonics, Ferroelectrics and Frequency Control, Vol. 58, No. 3, pp. 629-645, 2011.

23. Lee, S. and Youn, B. D., "A Design and Experimental Verification Methodology for an Energy Harvester Skin Structure," Smart Materials and Structures, Vol. 20, No. 5, Paper No. 057001, 2011.

24. De Marqui Junior, C., Erturk, A., and Inman, D. J., "An Electromechanical Finite Element Model for Piezoelectric Energy Harvester Plates," Journal of Sound and Vibration, Vol. 327, No. 1, pp. 9-25, 2009.

25. Rupp, C. J., Evgrafov, A., Maute, K., and Dunn, M. L., "Design of Piezoelectric Energy Harvesting Systems: a Topology Optimization Approach Based on Multilayer Plates and Shells," Journal of Intelligent Material Systems and Structures, Vol. 20, No. 16, pp. 1923-1939, 2009.

26. Institute, A. N. S., "IEEE Standard on Piezoelectricity: An American National Standard," Institute of Electrical and Electronics Engineers, 1988.

27. Jung, B. C., Yoon, H., Oh, H., Lee, G., Yoo, M., et al., "Hierarchical Model Calibration for Designing Piezoelectric Energy Harvester in the Presence of Variability in Material Properties and Geometry," Structural and Multidisciplinary Optimization, Vol. 53, No. 1, pp. 161-173, 2016.

28. Hu, C., Youn, B. D., and Yoon, H., "An Adaptive Dimension Decomposition and Reselection Method for Reliability Analysis," Structural and Multidisciplinary Optimization, Vol. 47, No. 3, pp. 423-440, 2013.

29. Upadrashta, D., Yang, Y., and Tang, L., "Material Strength Consideration in the Design Optimization of Nonlinear Energy Harvester," Journal of Intelligent Material Systems and Structures, Vol. 26, No. 15, pp. 1980-1994, 2015.

30. Bäck, T. and Schwefel, H.-P., "An Overview of Evolutionary Algorithms for Parameter Optimization," Evolutionary Computation, Vol. 1, No. 1, pp. 1-23, 1993.

31. Yildiz, A. R., "Comparison of Evolutionary-Based Optimization Algorithms for Structural Design Optimization," Engineering Applications of Artificial Intelligence, Vol. 26, No. 1, pp. 327-333, 2013.

32. Gunst, R. F., "Response Surface Methodology: Process and Product Optimization Using Designed Experiments," Taylor & Francis, 1996.

33. Huang, S.-C. and Dao, T.-P., "Design and Computational Optimization of a Flexure-Based XY Positioning Platform Using FEA-Based Response Surface Methodology," International Journal of Precision Engineering and Manufacturing, Vol. 17, No. 8, pp. 1035-1048, 2016.

34. Lee, H.-J., Park, S.-M., and Park, S.-J., "Minimization of Warpage for Wafer Level Package Using Response Surface Method," International Journal of Precision Engineering and Manufacturing, Vol. 17, No. 9, pp. 1201-1207, 2016.

35. Cho, S.-J., Cho, Y.-W., Lee, M. G., and Kim, J. H., "Variable Impact Analysis of Linear Generator by Using Response Surface Method," International Journal of Precision Engineering and Manufacturing, Vol. 17, No. 9, pp. 1223-1228, 2016.

36. Jin, R., Chen, W., and Simpson, T. W., "Comparative Studies of Metamodelling Techniques under Multiple Modelling Criteria," Structural and Multidisciplinary Optimization, Vol. 23, No. 1, pp. 1-13, 2001.

37. Wang, G. G. and Shan, S., "Review of Metamodeling Techniques in Support of Engineering Design Optimization," Journal of Mechanical Design, Vol. 129, No. 4, pp. 370-380, 2007.